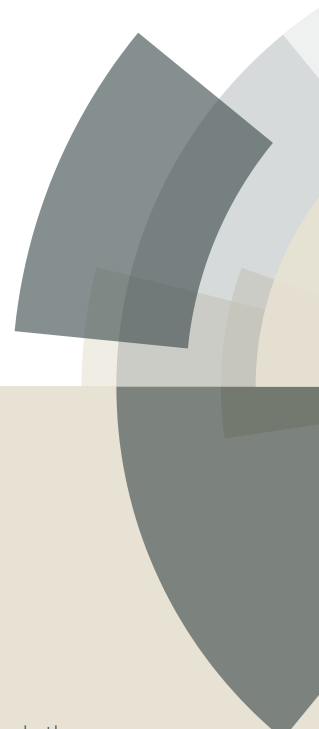


# PCCP

Accepted Manuscript



This article can be cited before page numbers have been issued, to do this please use: M. R. B, N. R. Chereddy, B. Shanigaram, B. Kotamarthi, S. Biswas, G. D. Sharma and J. R. Vaidya, *Phys. Chem. Chem. Phys.*, 2017, DOI: 10.1039/C7CP02729J.



This is an Accepted Manuscript, which has been through the Royal Society of Chemistry peer review process and has been accepted for publication.

Accepted Manuscripts are published online shortly after acceptance, before technical editing, formatting and proof reading. Using this free service, authors can make their results available to the community, in citable form, before we publish the edited article. We will replace this Accepted Manuscript with the edited and formatted Advance Article as soon as it is available.

You can find more information about Accepted Manuscripts in the [author guidelines](#).

Please note that technical editing may introduce minor changes to the text and/or graphics, which may alter content. The journal's standard [Terms & Conditions](#) and the ethical guidelines, outlined in our [author and reviewer resource centre](#), still apply. In no event shall the Royal Society of Chemistry be held responsible for any errors or omissions in this Accepted Manuscript or any consequences arising from the use of any information it contains.



Journal Name

ARTICLE

## Study on the effect of fluorine substitution on the photovoltaic properties of dithieno[3,2-*b*:2',3'-*d*]pyrrole-benzo[*c*][1,2,5]thiadiazole conjugate small molecule donor materials

Received 00th January 20xx,  
Accepted 00th January 20xx

DOI: 10.1039/x0xx00000x

www.rsc.org/

Manohar Reddy Busireddy,<sup>a</sup> Narendra Reddy Cherreddy,<sup>a,\*</sup> Balaiah Shanigaram,<sup>b</sup> Kotamarthi Bhanuprakash,<sup>b,\*</sup> Subhayan Biswas,<sup>c</sup> Ganesh Datt Sharma<sup>c,\*</sup> Vaidya Jayathirtha Rao<sup>a,d,\*</sup>

Two new small molecule donors namely **ICT4** and **ICT6** with D<sub>1</sub>-A-D<sub>2</sub>-A-D<sub>1</sub> architecture having 2,4-bis(2-ethylhexyl)-4*H*-dithieno[3,2-*b*:2',3'-*d*]pyrrole (EHDTP, D<sub>1</sub>) and ethylhexyloxybenzo[1,2-*b*:4,5-*b'*]dithiophene (OBDT, D<sub>2</sub>) as terminal and central donor and 4,8-bis((2- benzo[*c*][1,2,5]thiadiazole (BT for **ICT4**) and 5,6-difluorobenzo[*c*][1,2,5]thiadiazole (F2BT for **ICT6**) as acceptor (A) moieties are synthesized and their optical, electronic and photovoltaic properties are investigated. Both **ICT4** and **ICT6** are have considerable solubility in various solvents and possess efficient light absorption ability [ $\epsilon$  ( $\times 10^5 \text{ mol}^{-1} \text{ cm}^{-1}$ ) is 0.99 and 1.06, respectively for **ICT4** and **ICT6**) and appropriate frontier molecular orbital energy offsets with [6,6]-phenyl-C<sub>71</sub>-butyric acid methyl ester (PC<sub>71</sub>BM). Bulk heterojunction solar cells (BHJSCs) are fabricated using **ICT4/ICT6** and PC<sub>71</sub>BM as donor and acceptors, respectively and BHJSCs with the two step annealed (thermal followed by solvent vapor annealing) active layers of **ICT4** and **ICT6** shows overall power conversion efficiency (PCE) of 5.46 % and 7.91 %, respectively. Superior photovoltaic performance of **ICT6** based BHJSCs is due to the favourable morphology with nanoscale interpenetrating network in the **ICT6**:PC<sub>71</sub>BM active layer induced by the fluorine atoms on BT acceptor, which significantly enhances the dissociation of excitons, charge transport, charge collection efficiency and suppresses bimolecular recombination in the BHJ. Observed higher PCE of 7.91 % portray **ICT6** as one of the best BT based donor material for small molecular BHJSCs.

### Introduction

In recent years, organic bulk heterojunction solar cells (OBHJSCs) have been attracting immense interest from both industry and academia. Even though power conversion efficiencies (PCEs) reported for OBHJSCs are quite low than conventional silicon solar cells, former are advantageous in terms of their low production cost and simple fabricating procedures.<sup>1-3</sup> Generally, BHJ layer is a blend of electron

donating organic semiconductors (polymers or small molecules) and electron accepting fullerene derivatives. For OBHJSCs with polymer donor material, PCEs have been enhanced from below 1 % to over 10 % for single<sup>4-7</sup> and 12 % for multi-junction structure<sup>8,9</sup> by optimizing the donor materials molecular structure, BHJ morphology and device structure. However, intrinsic polydispersity associated with polymer donor materials due to batch-to-batch variation in their synthesis and difficulties in their purification and optimization of electronic properties intend to develop small molecule donor materials. Superior characteristics like simple synthesis, characterization and purification procedures associated with small molecule donor materials make them advantageous over their polymer counterparts.<sup>10,11</sup> Broader optical absorption for better exciton generation, suitable energy level offsets with fullerene acceptor for efficient dissociation of excitons and extended  $\pi$ -electron delocalization and planar backbone for high charge mobility are important for donor materials to obtain high PCEs.<sup>10-14</sup> Recently, PCE over 10 % has been reported for OBHJSCs with small molecule

<sup>a</sup>Crop Protection Chemicals Division, CSIR-Indian Institute of Chemical Technology, Hyderabad-500007, India. Email: [chereddynarendra@gmail.com](mailto:chereddynarendra@gmail.com); [vaidya.opv@gmail.com](mailto:vaidya.opv@gmail.com)

<sup>b</sup>Inorganic and Physical Chemistry Division, CSIR-Indian Institute of Chemical Technology, Hyderabad-500007, India

<sup>c</sup>Department of Physics, The LNM Institute of Information Technology, Jamdoli, Jaipur, India. Email: [gdsharma273@gmail.com](mailto:gdsharma273@gmail.com)

<sup>d</sup>AcSIR, CSIR-Indian Institute of Chemical Technology, Hyderabad-500007, India

† Footnotes relating to the title and/or authors should appear here.

Electronic Supplementary Information (ESI) available: [NMR, MALDI-MS, absorption and emission spectra and theoretical calculations] See DOI: 10.1039/x0xx00000x

donor materials.<sup>12-14</sup> However, PCE has to be improved further for commercial applications. Several new findings have been taking place in search of efficient donor/acceptor materials for OBHJSCs.<sup>15-22</sup> PCE of an OBHJSC can be enhanced by improving the magnitudes of short circuit current density ( $J_{sc}$ ), open-circuit voltage ( $V_{oc}$ ) and fill factor (FF) of the devices. Generally,  $J_{sc}$  of an OBHJSC can be increased by exploiting donor materials with efficient light harvesting capacity and  $V_{oc}$  can be improved by lowering their HOMO energy to reduce the exciton recombination.<sup>23,24</sup>

From our recent findings, we observed that incorporation of dithieno[3,2-*b*:2',3'-*d*]pyrrole (DTP) donor moiety can impart intense visible and NIR absorption to donor materials.<sup>25,26</sup> Moreover, recent reports revealed that attachment of fluorine atoms to the molecular backbone of donor materials can lower down their HOMO energy and thereby improves the  $V_{oc}$  of OBHJSCs and as well as fluorine atoms at appropriate location of donor materials can improve  $J_{sc}$  and FF of the devices.<sup>27-30</sup>

Extensive studies have been carried out to comprehend the influence of fluorination on photovoltaic properties of benzo[*c*][1,2,5]thiadiazole (BT) based polymer donor materials.<sup>28,21-42</sup> However, efforts to demonstrate the importance of fluorination to obtain efficient BT based small molecule donor materials are relatively low.<sup>43-49</sup>

Considering all the factors mentioned above, we have synthesized two new small molecule donors, **ICT4** and **ICT6** with subtle variations in their structure. Synthesized donor materials have D<sub>1</sub>-A-D<sub>2</sub>-A-D<sub>1</sub> linear architecture containing 2,4-bis(2-ethylhexyl)-4*H*-dithieno[3,2-*b*:2',3'-*d*]pyrrole (EHDP) terminal donor (D<sub>1</sub>), BT with different extents of fluorine substitution (BT for **ICT4** and F2BT for **ICT6**) and 4,8-bis((2-ethylhexyl)oxy)benzo[1,2-*b*:4,5-*b'*]dithiophene (OBDT) as acceptor (A) and central donor (D<sub>2</sub>) moieties, respectively. We choose OBDT as central donor owing to its excellent properties. With a flat and three ring fused structure, BDT can trigger efficient intermolecular interactions among the donor molecules in their thin films and there by enhances the charge carrier dynamics in the BHJ.<sup>13,14,50-53</sup> BT with different degrees of fluorine substitution are selected as acceptor moieties to explore the effects of fluorine atoms on BT acceptor moieties of the synthesized EHDP end-capped donor molecules on their thermal, photophysical, electrochemical and photovoltaic properties. Excellent thermal stability, efficient light harvesting ability of **ICT4** and **ICT6** and their appropriate frontier molecular orbital energy levels compared to [6,6]-phenyl-C<sub>71</sub>-butyric acid methyl ester (PC<sub>71</sub>BM) portray them as suitable donors for BHJSCs employing PC<sub>71</sub>BM acceptor. A detailed structural analysis of donor materials in BHJ thin films has been carried out using X-ray diffraction and transmission electron microscope analyses to understand how morphology of the BHJ changes with fluorine atom substitution. Also influence of fluorine atom substitution on various photovoltaic parameters of their BHJSCs is explained in detail. To our knowledge, this is the first report demonstrating the influence of fluorine substitution on optical, electronic and photovoltaic properties of BT-DTP conjugate small molecule donors.

## Experimental Section

### Materials and instruments

Synthetic precursors reported in this study are obtained either directly from commercial suppliers or synthesized as per the literature procedures. All the experiments are performed using dry organic solvents. NMR spectral analysis is carried out on Bruker Avance (500 MHz) spectrometer and MALDI-MS data is acquired using a Thermofinnigan mass spectrometer. Absorption measurements are performed on a Cary 5000 UV-VIS-NIR spectrophotometer. Fluorescence experiments are carried out on Cary Eclipse fluorescence spectrophotometer and Horiba Jobin Yvon Fluorolog Fluorimeter. Cyclic voltammetry measurements, thermogravimetric analysis and differential scanning calorimetry experiments are conducted as previously described.<sup>17</sup>

### BHJSC device studies

BHJSCs with indium tin oxide (ITO)/poly(3,4-ethylenedioxythiophene):polystyrene sulfonate (PEDOT:PSS)/**ICT4** or **ICT6**:PC<sub>71</sub>BM/poly[(9,9-bis(3'-(*N,N*-dimethylamino)propyl)fluorene-2,7-diyl)-*alt*-(9,9-dioctylfluorene-2,7-diyl) (PFN)/aluminum (Al) architecture are fabricated as follows: First of all the ITO coated glass substrates are pre-cleaned in ultrasonicator containing de-ionized water, acetone and iso-propanol, sequentially for 20 minutes each followed by UV/ozone treatment for 1 h to remove organic residues. PEDOT:PSS is layered (thickness of ~40 nm) on the pre-cleaned ITO coated glass substrate using a spin coater and dried at 120 °C for 20 minutes. On the top of the ITO/PEDOT:PSS, active layer is spin coated from the blend solution (chloroform solvent) consisting of different weight ratios of donor (**ICT4** or **ICT6**) and PC<sub>71</sub>BM, keeping its total concentration as 16 mg/mL. Active layer coated plates are dried at 50 °C for 10 minutes to remove the organic residue. Two-step annealing (TSA) process has been carried out by annealing the active layer coated ITO glass substrates at 120 °C for 10 minutes, followed cooling to RT and subsequently keeping them for 10 minutes in a Petri dish present in a THF contained chamber. A layer of PFN (thickness of ~5 nm) is spin coated onto the active layer from its methanol solution. Finally an aluminum (Al) electrode is deposited using thermal evaporation technique under a vacuum of 1 × 10<sup>-6</sup> Torr. The shadow mark method is used to define the effective area of the fabricated devices and is about 16 mm<sup>2</sup>. The devices are characterized at ambient conditions under AM1.5 G stimulated solar illumination (100 mW/cm<sup>2</sup>) using a xenon lamp based solar simulator. The current-voltage (J-V) characteristics of the fabricated devices are measured on a Keithley source meter unit controlled by a PC. The incident photon to current efficiency (IPCE) characteristics of the fabricated devices is studied under short circuit conditions using a Keithley electrometer. Devices are illuminated with light source and monochromator and resulting current is collected using the electrometer unit.

### Synthetic procedures

Intermediates, *N,N*-diethylthiophene-3-carboxamide (**1**), 4,8-dihydrobenzo[1,2-*b*:4,5-*b'*]dithiophene-4,8-dione (**2**), 4,8-bis((2-ethylhexyl)oxy)benzo[1,2-*b*:4,5-*b'*]dithiophene (**3**), (4,8-bis((2-ethylhexyl)oxy)benzo[1,2-*b*:4,5-*b'*]dithiophene-2,6-diyl)bis(trimethylstannane) (**4**), 3,3'-dibromo-2,2'-dithiophene (**5**), *N*-(2-ethylhexyl)-4*H*-dithieno[3,2-*b*:2',3'-*d'*]pyrrole (**6**) are synthesized as per our previously reported procedures.<sup>25</sup>

#### 2,4-bis(2-ethylhexyl)-4*H*-dithieno[3,2-*b*:2',3'-*d'*]pyrrole (**7**):

Compound **6** (0.73 g, 2.5 mmol) and dry THF (30 mL) are added to a double necked RB flask dried over flame and maintained at -78 °C under N<sub>2</sub> atmosphere. *n*-BuLi (2.5 M in hexanes, 2.75 mmol, 1.1 mL) is slowly added to the solution and stirred for 1 h at -78 °C followed by adding 2-ethylhexyl bromide (0.5 mL, 2.8 mmol). Resultant solution is stirred at RT overnight, added with ice water (20 mL) and the layers formed are separated. The aqueous layer collected is washed with chloroform (3 x 10 mL) and all the organic portions are combined, dried using anhydrous Na<sub>2</sub>SO<sub>4</sub> and filtered. Filtrate obtained is concentrated using a rotary evaporator and the residue formed is purified using a silica gel column (eluent: hexane) to acquire the desired product as a colorless oil (yield 75%).

<sup>1</sup>H NMR (500 MHz, CDCl<sub>3</sub>, δ ppm): 0.82-0.95 (m, 12H), 1.22-1.43 (m, 16H), 1.56-1.69 (m, 1H), 1.86-1.97 (m, 1H), 2.80 (d, *J* = 7.0 Hz, 2H), 3.95-4.05 (m, 2H), 6.66 (s, 1H), 6.94 (d, *J* = 6.0 Hz, 1H), 7.03 (d, *J* = 6.0 Hz, 1H); <sup>13</sup>C NMR (125 MHz, CDCl<sub>3</sub>, δ ppm): 10.67, 10.86, 14.00, 14.13, 22.97, 23.02, 24.01, 25.58, 28.64, 28.85, 30.65, 32.36, 35.56, 40.45, 41.53, 51.19, 109.34, 110.96, 112.37, 114.98, 121.47, 142.69, 143.84, 144.43.

#### 2,4-bis(2-ethylhexyl)-6-(trimethylstannyl)-4*H*-dithieno[3,2-*b*:2',3'-*d'*]pyrrole (**8**):

Under N<sub>2</sub> atmosphere, *n*-BuLi (2.5 M in hexanes, 2.75 mmol, 1.1 mL) is slowly added to the dry THF (25 mL) solution of **7** (1.0 g, 2.5 mmol) maintaining at -78 °C and stirred for 1 h. Trimethyltin chloride in hexane (1 M, 2.75 mL, 2.75 mmol) is injected into the reaction vessel and the solution is allowed to reach RT and stirred overnight. Reaction mixture is added with ice water (20 mL) and washed with diethyl ether (3 x 20 mL). All the organic fractions are combined and dried using anhydrous Na<sub>2</sub>SO<sub>4</sub>. Filtrate obtained upon filtration of this solution is concentrated using a rotary evaporator to achieve the desired product as light brown oil (yield 82%).

<sup>1</sup>H NMR (500 MHz, CDCl<sub>3</sub>, δ ppm): 0.39 (s, 9H), 0.85-0.93 (m, 12H), 1.25-1.39 (m, 16H), 1.59-1.66 (m, 1H), 1.89-1.98 (m, 1H), 2.79 (d, *J* = 7.0 Hz, 2H), 3.96-4.05 (m, 2H), 6.64 (s, 1H), 6.95 (s, 1H); <sup>13</sup>C NMR (125 MHz, CDCl<sub>3</sub>, δ ppm): -8.16, 10.69, 10.88, 14.04, 14.13, 23.01, 23.99, 25.61, 28.55, 28.85, 28.88, 30.58, 32.37, 35.60, 40.40, 41.55, 51.12, 109.41, 112.43, 117.89, 120.50, 134.34, 142.49, 144.72, 146.58..

#### 2-(7-bromobenzo[*c*][1,2,5]thiadiazol-4-yl)-4,6-bis(2-ethylhexyl)-4*H*-dithieno[3,2-*b*:2',3'-*d'*]pyrrole (**9**)

To a thoroughly dried double necked RB flask, BrBT<sup>42</sup> (0.29 g, 1 mmol), **8** (0.57 g, 1 mmol) and tetrakis(triphenylphosphine)palladium (58 mg, 0.05 mmol) are

added and connected to a reflux condenser. Dry toluene (10 mL) is injected into the RB flask and the reaction mixture is bubbled with N<sub>2</sub> for 20 minutes. Resulting solution is heated and stirred overnight at reflux temperature. On the next day, reaction mixture is cooled down to RT, added with chloroform (20 mL) and filtered through celite bed. Filtrate obtained is partitioned between chloroform and water and organic portion is collected. Aqueous portion is washed with chloroform (3 x 10 mL) and all the organic portions are combined, dried using anhydrous Na<sub>2</sub>SO<sub>4</sub> and filtered. Filtrate obtained is concentrated using a rotary evaporator and the residue formed is purified using a silica gel column (eluent: chloroform/petroleum ether, 1:6 v/v) to obtain **9** as a red solid (yield 75%).

<sup>1</sup>H NMR (500 MHz, CDCl<sub>3</sub>, δ ppm): 0.85-0.98 (m, 12H), 1.26-1.44 (m, 16H), 1.62-1.70 (m, 1H), 1.94-2.04 (m, 1H), 2.82 (d, *J* = 7.0 Hz, 2H), 4.03-4.17 (m, 2H), 6.68 (s, 1H), 7.66 (d, *J* = 7.5 Hz, 1H), 7.80 (d, *J* = 8.0 Hz, 1H), 8.28 (s, 1H); <sup>13</sup>C NMR (125 MHz, CDCl<sub>3</sub>, δ ppm): 10.74, 10.86, 14.09, 14.14, 22.97, 23.02, 24.09, 25.60, 28.61, 28.86, 30.63, 32.38, 35.75, 40.45, 41.50, 51.12, 109.33, 110.40, 112.76, 113.22, 116.09, 123.78, 128.50, 132.33, 134.40, 144.70, 145.01, 145.69, 151.61, 153.89.

#### 2-(7-bromo-5,6-difluorobenzo[*c*][1,2,5]thiadiazol-4-yl)-4,6-bis(2-ethylhexyl)-4*H*-dithieno[3,2-*b*:2',3'-*d'*]pyrrole (**10**)

Similar procedure used to synthesize **9** is adopted to obtain **10** using BrF<sub>2</sub>BT<sup>30</sup> and **8** as the as synthetic precursors (yield 76%). <sup>1</sup>H NMR (500 MHz, CDCl<sub>3</sub>, δ ppm): 0.85-0.97 (m, 12H), 1.25-1.44 (m, 16H), 1.60-1.73 (m, 1H), 1.89-2.02 (m, 1H), 2.82 (d, *J* = 8.0 Hz, 2H), 4.00-4.13 (m, 2H), 6.67 (s, 1H), 8.25 (s, 1H); <sup>13</sup>C NMR (125 MHz, CDCl<sub>3</sub>, δ ppm): 10.65, 10.80, 14.03, 14.08, 22.89, 22.96, 24.04, 25.55, 28.53, 28.76, 30.53, 32.32, 35.67, 40.33, 41.39, 50.84, 109.12, 112.60, 112.87, 113.18, 113.81, 116.95, 128.31, 128.50, 128.60, 130.07, 132.81, 144.36, 145.59, 146.05, 148.44, 153.92, 153.99, 159.29, 161.78.

#### 6,6'-(7,7'-(4,8-bis((2-ethylhexyl)oxy)benzo[1,2-*b*:4,5-*b'*]dithiophene-2,6-diyl)bis(benzo[*c*][1,2,5]thiadiazole-7,4-diyl))bis(2,4-bis(2-ethylhexyl)-4*H*-dithieno[3,2-*b*:2',3'-*d'*]pyrrole) (ICT4)

To a thoroughly dried double necked RB flask (50 mL) connected to a reflux condenser, **4** (0.38 g, 0.5 mmol), **9** (0.93 g, 1.5 mmol) and tetrakis(triphenylphosphine)palladium (58 mg, 0.05 mmol) and dry toluene (10 mL) are added and the solution is bubbled with N<sub>2</sub> gas for 20 minutes. Resulting solution is heated, stirred overnight at reflux temperature and the reaction progress is monitored using TLC. After complete consumption of **4**, reaction mixture is cooled down to RT and chloroform (20 mL) is added. Solution obtained is filtered through celite bed. Filtrate is washed with water and the aqueous phase is extracted with chloroform (2 x 20 mL). All the organic fractions are combined and dried using anhydrous Na<sub>2</sub>SO<sub>4</sub>. The resultant solution is filtered, filtrate obtained is concentrated using a rotary evaporator and the residue formed is purified using a silica gel column (eluent:

chloroform/petroleum ether, 1:6 v/v) to yield **ICT4** as a blue-black solid (yield 72%).

$^1\text{H}$  NMR (500 MHz,  $\text{CDCl}_3$ ,  $\delta$  ppm): 0.83-0.98 (m, 24H), 1.05-1.14 (m, 6H), 1.21-1.45 (m, 36H), 1.55-1.92 (m, 24H), 2.74 (d,  $J = 7.0$  Hz, 4H), 3.56-3.71 (m, 4H), 4.20 (s, 4H), 6.43 (s, 2H), 7.30-7.53 (m, 4H), 8.01 (s, 2H), 8.48 (s, 2H);  $^{13}\text{C}$  NMR (125 MHz,  $\text{CDCl}_3$ ,  $\delta$  ppm): 10.99, 11.08, 11.96, 14.40, 14.72, 23.24, 23.32, 23.67, 24.33, 25.83, 28.87, 29.08, 29.12, 29.77, 29.94, 30.87, 31.01, 32.66, 35.96, 40.63, 41.11, 41.72, 50.76, 75.66, 109.51, 112.85, 112.97, 115.82, 121.81, 122.91, 124.06, 126.71, 127.58, 128.88, 133.25, 135.72, 138.63, 144.31, 144.40, 145.00, 145.63, 152.19, 152.67.

MALDI-MS (Positive mode,  $m/z$ ): 1516.66 ( $\text{M}^+$ ), Calc. for  $\text{C}_{86}\text{H}_{112}\text{N}_6\text{O}_2\text{S}_8$  is 1516.66.

### 6,6'-(7,7'-(4,8-bis((2-ethylhexyl)oxy)benzo[1,2-*b*:4,5-*b'*])dithiophene-2,6-diyl)bis(5,6-difluorobenzo[*c*][1,2,5]thiadiazole-7,4-diyl)bis(2,4-bis(2-ethylhexyl)-4*H*-dithieno[3,2-*b*:2',3'-*d*]pyrrole) (**ICT6**)

**ICT6** is synthesized as per the procedure described for **ICT4** using **4** and **10** as synthetic precursors (yield 75%).

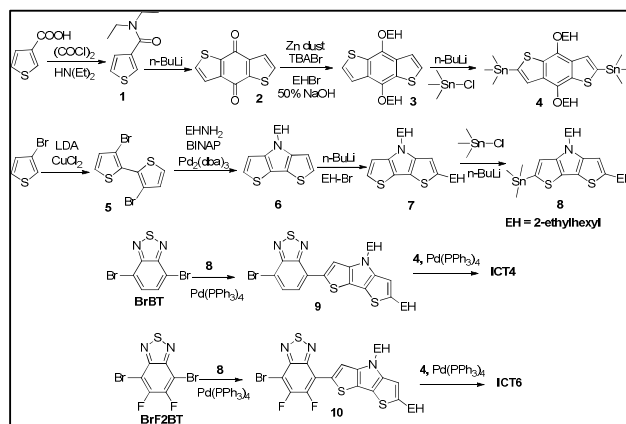
$^1\text{H}$  NMR (500 MHz,  $\text{CDCl}_3$ ,  $\delta$  ppm): 0.76-0.88 (m, 12H), 0.90-0.98 (m, 12H), 1.10-1.16 (m, 6H), 1.21-1.41 (m, 36H), 1.57-1.96 (m, 24H), 2.44 (d,  $J = 7.0$  Hz, 4H), 3.77-3.96 (m, 4H), 4.22 (s, 4H), 6.26 (s, 2H), 7.96 (s, 2H), 8.33 (s, 2H);  $^{13}\text{C}$  NMR (125 MHz,  $\text{CDCl}_3$ ,  $\delta$  ppm):  $^{13}\text{C}$  NMR (125 MHz,  $\text{CDCl}_3$ ,  $\delta$  ppm): 10.77, 10.80, 11.69, 14.15, 14.44, 23.04, 23.40, 24.13, 25.56, 28.64, 28.80, 28.83, 29.54, 29.68, 29.71, 30.66, 30.82, 32.37, 35.67, 40.42, 40.90, 41.44, 50.73, 75.35, 109.13, 109.41, 109.55, 112.61, 113.36, 1132.50, 113.82, 116.74, 122.89, 122.96, 127.22, 127.32, 129.73, 129.80, 131.84, 132.38, 132.45, 133.85, 143.92, 144.62, 145.02, 145.92, 149.28, 153.34, 153.45, 158.42, 160.95.

MALDI-MS (Positive mode,  $m/z$ ): 1588.66 ( $\text{M}^+$ ), Calc. for  $\text{C}_{86}\text{H}_{108}\text{F}_4\text{N}_6\text{O}_2\text{S}_8$  is 1588.62.

## Results and discussion

### Synthesis and thermal properties

Structures of **ICT4** and **ICT6** is presented in Fig. S1, ESI<sup>†</sup> and scheme for their synthesis is provided in **scheme 1**. **ICT4** and **ICT6** are obtained from their corresponding mono-bromo derivatives (**9** and **10**, respectively for **ICT4** and **ICT6**) by reacting with distannyl intermediate **4** under Stille coupling protocol. Mono-bromo intermediates **9** and **10** are obtained from their corresponding dibromobenzothiadiazole precursors (BrBT for **ICT4** and BrF2BT for **ICT6**) by reacting with stannyl DTP derivative **8**, which is obtained by reacting **7** with trimethyltin chloride and *n*-BuLi. Intermediate **7** is synthesized by reacting **6** with *n*-BuLi and 2-ethylhexyl bromide. Intermediates **1**, **2**, **3**, **4**, **5** and **6** are synthesized as per our previous procedures.<sup>25</sup> Dibromobenzothiadiazole precursors (BrBT and BrF2BT) are synthesized as per the procedures available in the literature.<sup>49,39</sup> Both **ICT4** and **ICT6** have fair solubility in various organic solvents (>25 mg/mL). However, solubility of **ICT6** having four fluorine atoms is lesser than **ICT4**.



**Scheme 1.** Synthetic scheme of **ICT4** and **ICT6**.

Through characterization of **ICT4** and **ICT6** has been done using NMR and MALDI-MS analyses (Figs. S2-S7, ESI<sup>†</sup>).

To evaluate the thermal characteristics of **ICT4** and **ICT6**, thermogravimetry (TGA) and differential scanning calorimetry (DSC) analyses are performed and the obtained results are presented in **Fig. 1** (**Fig. 1a** and **Fig. 1b** are corresponding to TGA and DSC analyses, respectively) and Table 1. Elevated decomposition temperatures ( $T_d$ ) of **ICT4** and **ICT6** obtained from TGA, confirms their superior thermal stability (**Fig. 1a** and Table 1). Similar  $T_d$  values of **ICT4** (342 °C) and **ICT6** (344 °C) indicates that fluorination of the BT acceptor unit has minimal impact on their thermal degradation. Both **ICT4** and **ICT6** display glass transition temperatures (124 and 119 °C, respectively for **ICT4** and **ICT6**) during the second heating cycle of their DSC analysis (**Fig. 1b**). Such a phase transition can induce significant changes in their morphology upon thermal or solvent vapor annealing processes during device fabrication.<sup>54</sup> Melting ( $T_m$ ) and crystallization ( $T_c$ ) temperatures of **ICT4** and **ICT6** are also estimated from DSC analysis (**Fig. 1b** and Table 1). Contrary to the thermal degradation, extent of fluorine atoms has significant impact on their  $T_m$  and  $T_c$  values. **ICT4** shows clear melting ( $T_m$ ) and crystallization ( $T_c$ ) thermograms at 260 and 249 °C, respectively. However, **ICT6** with four fluorine atoms does not show any melting or crystallization behavior in the operated temperature range, indicating its higher melting and crystallization temperatures.

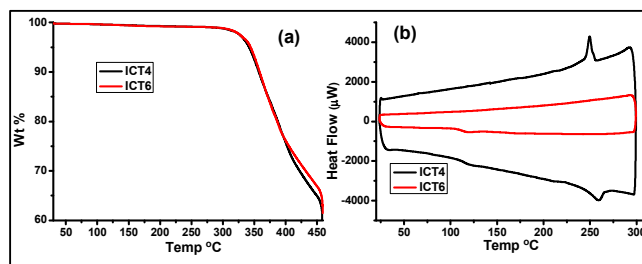


**Fig. 1.** Thermograms of **ICT4** and **ICT6** obtained from TGA (a) and DSC (b) analysis

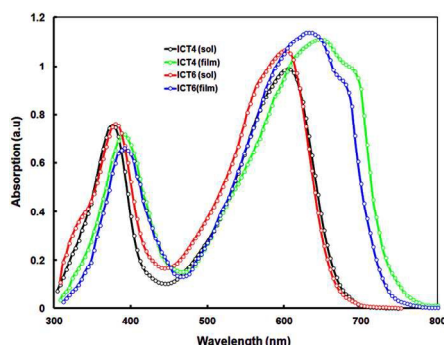


**Fig. 2.** Solution (chloroform, 10  $\mu$ M) and thin film state absorption spectra of **ICT4** and **ICT6**.

Observed higher  $T_m$  and  $T_c$  values could be due to strong intermolecular interactions associated with the fluorine atom substituted donor material **ICT6**.<sup>55,56</sup> High  $T_d$  and  $T_m$  values of the **ICT4** and **ICT6** reveals their suitability for application even at elevated temperatures.

### Photo-physical and electrochemical properties

Absorption spectra of **ICT4** and **ICT6** in solution and thin films are presented in **Fig. 2** and relevant data is given in Table 2. In chloroform solution, **ICT4** and **ICT6** display absorption bands in two distinct regions i.e 300-450 nm and 450-700 nm, respectively. Compared to **ICT4**, longer wavelength absorption band of **ICT6** is faintly blue shifted and concomitant increase in molar extinction coefficient ( $\epsilon$ ) is observed (**Fig. 2**). Enhancement in  $\epsilon$  of **ICT6** could be due to improvement in its molecular backbone planarity.<sup>57,58</sup> Absorption bands of **ICT4** and **ICT6** are red shifted in their thin film state with a new vibronic shoulder peak at longer wavelength regions (**Fig. 2**), indicating the strong intermolecular interactions due to  $\pi$ -stacking and efficient intermolecular packing between the molecular backbones.<sup>46,47</sup> Onset of thin film absorption spectra is used to estimate the optical band gap of **ICT4** and **ICT6**. To estimate HOMO (highest occupied molecular orbital) and LUMO (lowest unoccupied molecular orbital) energies of **ICT4** and **ICT6**, we have measured their electrochemical properties using cyclic voltammetry (CV) analysis. Cyclic voltammograms representing the reduction behavior of **ICT4** and **ICT6** are given in **Fig. S8**, ESI<sup>†</sup> and relevant data is provided in Table 2. Compared to **ICT4**, **ICT6** shows decreased reduction potential and it could be due to strong electron accepting tendency of fluorine (**Fig. S8a**, ESI<sup>†</sup> and Table 2). LUMO energy of **ICT4** and

**Table 1.** Thermal data of **ICT4** and **ICT6**.

Material	Decomposition temperature ( $T_d$ ) <sup>o</sup> C	Glass transition temperature ( $T_g$ ) <sup>o</sup> C	Melting temperature ( $T_m$ ) <sup>o</sup> C	Crystallization temperature ( $T_c$ ) <sup>o</sup> C
<b>ICT4</b>	342	124	260	249
<b>ICT6</b>	344	119	-	-

**Table 2.** Photophysical and electrochemical data of **ICT4** and **ICT6**.

Material	$\lambda_{max}$ (nm) <sup>a</sup>	$\epsilon$ ( $\times 10^4$ mol <sup>-1</sup> cm <sup>-1</sup> ) <sup>a</sup>	$\lambda_{max}$ (nm) <sup>b</sup>	$E_{o-o}$ (eV) <sup>c</sup>	$E_{red}$ (V)	$E_{HOMO}$ (eV) <sup>d</sup>	$E_{LUMO}$ (eV)
<b>ICT4</b>	604	0.99	652	1.90	-1.43	-5.55	-3.65
<b>ICT6</b>	596	1.06	636	1.97	-1.36	-5.66	-3.69

<sup>a</sup>in solution (chloroform, 10  $\mu$ M), <sup>b</sup>in thin film (cast from chloroform solution), <sup>c</sup>calculated from the absorption and emission spectra intersection point, <sup>d</sup> $E_{HOMO} = E_{LUMO} + E_g^{opt}$ .

**ICT6** is measured using their onset reduction potential obtained from CV analysis (Table 2) and their HOMO energy is calculated using  $E_{HOMO} = E_{LUMO} + E_g^{opt}$  [ $E_g^{opt}$  is the optical band gap, measured from the intersection wavelength of donor materials solution state absorption and emission spectra (**Fig. S9**, ESI<sup>†</sup>)]. Introduction of fluorine atoms significantly lowers down the HOMO energy of **ICT6** (Table 2). Since the  $V_{oc}$  of BHJSC depends on the energy difference between the donor HOMO and acceptor LUMO, observed deep-lying HOMO energy of **ICT6** can bestow high  $V_{oc}$  for their corresponding BHJSCs. The frontier molecular orbital energy levels of **ICT4** and **ICT6** are well aligned with HOMO (-6.1 eV) and LUMO (-4.3 eV) energies of PC<sub>71</sub>BM (**Fig. S10**, ESI<sup>†</sup>). This indicates the applicability of **ICT4** and **ICT6** as donors for BHJSCs with PC<sub>71</sub>BM acceptor. The higher magnitude energy gap between the LUMO of **ICT4/ICT6** and PC<sub>71</sub>BM over the threshold value (0.3 eV) reported for effective dissociation of excitons into free charge carriers indicates efficient exciton dissociation at **ICT4/ICT6** and PC<sub>71</sub>BM junction.<sup>59</sup>

To understand the photo-induced charge transfer characteristics between **ICT4/ICT6** and PC<sub>71</sub>BM, photoluminescence (PL) of pure donor materials and their blend films with PC<sub>71</sub>BM are measured by exciting at 580 nm (**Fig. S8b**, ESI<sup>†</sup>). As presented in **Fig. S8b**, ESI<sup>†</sup>, blend film of **ICT6/PC<sub>71</sub>BM** demonstrate about 92 % PL quenching in comparison with the PL spectrum of pristine **ICT6**, which is higher than that of **ICT4:PC<sub>71</sub>BM** blend film (83 %). These results indicate that pronounced photo-induced charge transfer can occur between **ICT6** and PC<sub>71</sub>BM compared to **ICT4** and PC<sub>71</sub>BM, and indicates **ICT6** as more suitable small molecule donor for PC<sub>71</sub>BM acceptor for the application in BHJSCs.

### Theoretical studies

Theoretical studies are performed using Gaussian 09 package (B3LYP functional along with 6-31G(d,p) basis set for DFT and M06-2X functional and 6-311G(d,p) basis set for TD-DFT) and detailed procedures described in our previous report.<sup>25</sup> Various conformations of **ICT4** and **ICT6** are optimized and the conformer with lowest energy is used for theoretical calculations (**Fig. S11**, ESI<sup>†</sup>). Optimized structures of **ICT4** and **ICT6** is presented in **Fig. S12**, ESI<sup>†</sup>. Both **ICT4** and **ICT6** are almost planar with zero dipole moment. The dihedral angle between OBDT and outer BT-EHDTP or F2BT-EHDTP molecular planes are in the range of 0.06 - 4.54 $^\circ$  and 0.09 - 2.51 $^\circ$  for **ICT4**

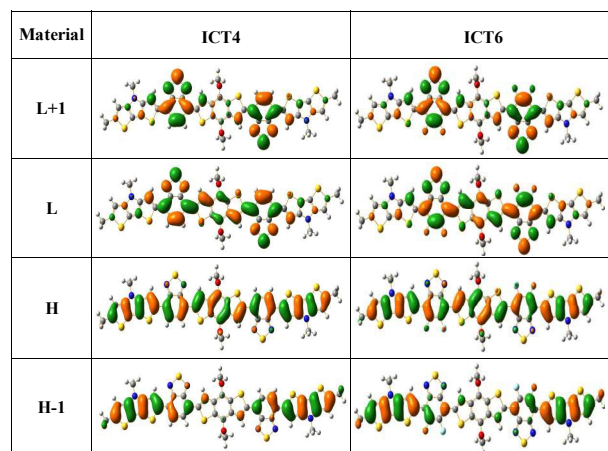


Fig. 3. FMO distributions of ICT4 and ICT6

and ICT6, respectively indicating high planarity of ICT6. High planarity generally improves intramolecular electron delocalization and enhances molar extinction coefficient of the electronic transition and it is well supported by the observed high  $\epsilon$  values of ICT6 over ICT4 (Fig. 2). Calculated HOMO (H) and LUMO(L) energies, allowed vertical electronic excitation and optical band gaps using M06-2X functional are given in Tables S1, ESI<sup>†</sup>. The first excitation neatly shows a strong single-configuration nature (H to L) with a moderate secondary (H-1 to L+1). Isosurface plots (isovalue 0.02) of the H-1, H, L and L+1 orbitals of the ICT4 and ICT6 are illustrated in Fig. 3. For both ICT4 and ICT6, HOMO is extended over all the fragments of donor molecules and LUMO is distributed over the BT-OBDBT-BT (ICT4), F2BT-OBDBT-F2BDT (ICT6) moieties, indicating intramolecular charge transfer from EHDP moiety to BT or F2BT moieties. However, H-1 and L+1 does not exhibit significant contributions from OBDBT moieties, but are rather localized mainly towards EHDP and BT or F2BT moieties.

Absorption spectra simulated by TD-DFT of ICT4 and ICT6 using M06-2X/6-311G(d, p) in chloroform solvent are given in Fig. S13, ESI<sup>†</sup>. GaussSum 3.0 software is used to convolute Gaussian function to produce spectra with a FWHM value of 3000  $\text{cm}^{-1}$ . Calculated spectra are in line with experimental obtained. Though, absorption maxima values are slightly underestimated by about 40 nm using M06-2X functional. Excitation wavelengths corresponding to the strongest oscillator strengths observed for these band values are given in Table S1, ESI<sup>†</sup>.

### Photovoltaic properties

BHJSCs with conventional structure ITO/PEDOT:PSS/ICT4 or ICT6:PC<sub>71</sub>BM/PFN/Al are fabricated and characterized under AM1.5 solar illumination (100  $\text{mW}/\text{cm}^2$ ). PFN is employed as cathode interface to improve photovoltaic performance of the devices. First of all, we have optimized the donor to acceptor weight ratio (1:1, 1:1.5 1:2 and 1:2.5) in chloroform solution and best photovoltaic performance is achieved with 1:2 D/A weight ratio. The current-voltage (J-V) characteristics of the optimized devices and corresponding photovoltaic parameters

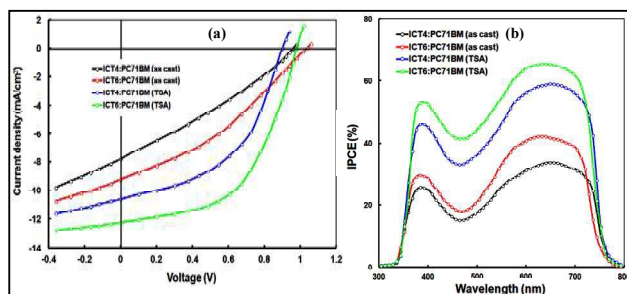


Fig. 4. J-V characteristics (a) under illumination and IPCE spectra (b) of the devices under different conditions.

are provided Fig. 4a and Table 3, respectively. Without any treatment, BHJSC with ICT4 donor shows only a PCE of 2.70 % with  $J_{\text{SC}}$  of 7.82  $\text{mA}/\text{cm}^2$ ,  $V_{\text{OC}}$  of 0.96 V and FF of 0.36. Under same conditions, BHJSC with ICT6 shows PCE of 3.84 % with  $J_{\text{SC}}$  of 9.24  $\text{mA}/\text{cm}^2$ ,  $V_{\text{OC}}$  of 1.04 V and FF of 0.40. Higher  $V_{\text{OC}}$  values associated for both the devices could be due to the low lying HOMO of donor materials. Since the  $V_{\text{OC}}$  values of these devices are significant, low PCE of these devices is mainly related to their poor  $J_{\text{SC}}$  and FF values and it could be due to inappropriate nanoscale morphology of the BHJ. After the two step annealing process (TSA), photovoltaic performance of the BHJSCs with ICT4 and ICT6 donors is improved significantly i.e. 5.46 % and 7.91 %, respectively. IPCE spectra of the BHJSCs with active layers processed under different conditions are shown in Fig. 4b. IPCE values for BHJSCs with TSA treated active layer are significantly higher over their as cast counterparts contributing to increase in their  $J_{\text{SC}}$  values. J-V characteristics (Fig. 4a) reveals that BHJSCs with the active layer containing ICT6 donor processed under TSA conditions have superior  $V_{\text{OC}}$ ,  $J_{\text{SC}}$  and FF values ( $J_{\text{SC}} = 12.23 \text{ mA}/\text{cm}^2$ ,  $V_{\text{OC}} = 0.98 \text{ V}$  and FF = 0.66) over the devices with ICT4 active layer ( $J_{\text{SC}} = 10.52 \text{ mA}/\text{cm}^2$ ,  $V_{\text{OC}} = 0.91 \text{ V}$  and FF = 0.57). As ICT6 has deeper HOMO level than ICT4, higher  $V_{\text{OC}}$  for the devices with ICT6 is expected. To understand the rationale for higher photovoltaic efficiency of ICT6 based devices, we have carried out further investigations including IPCE response, charge transport and morphology of BHJ thin films. The IPCE spectra of the BHJSCs with ICT4:PC<sub>71</sub>BM and ICT6:PC<sub>71</sub>BM BHJ are presented in Fig. 4b. Both the devices shows wide response ranging from 350 to 750 nm. However, the device with ICT6 active layer shows higher IPCE maximum value (67 %) over the

Table 3. Photovoltaic parameters observed for BHJSCs with ICT4/ICT6 donor and PC<sub>71</sub>BM acceptor

Active layer	$J_{\text{SC}}$ ( $\text{mA}/\text{cm}^2$ )	$V_{\text{OC}}$ (V)	FF	PCE (%)
ICT4:PC <sub>71</sub> BM (as cast)	7.82	0.96	0.36	2.70 (2.62) <sup>a</sup>
ICT6:PC <sub>71</sub> BM (as cast)	9.24	1.04	0.40	3.84 (3.71) <sup>a</sup>
ICT4:PC <sub>71</sub> BM (TSA)	10.52	0.91	0.57	5.46 (5.37) <sup>a</sup>
ICT6:PC <sub>71</sub> BM (TSA)	12.23	0.98	0.66	7.91 (7.83) <sup>a</sup>

<sup>a</sup>Average of 8 devices

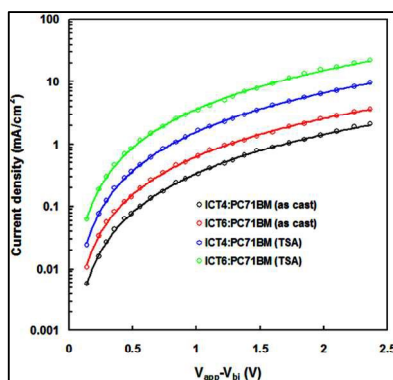


Fig. 5 J–V characteristics in the dark for hole-only devices with active layers processed under different conditions

device with **ICT4** active layer (54%) and it could be responsible for the higher  $J_{SC}$  value observed for **ICT6** based devices. The  $J_{SC}$  values calculated from the integration of IPCE spectra are 10.41 mA/cm<sup>2</sup> and 12.13 mA/cm<sup>2</sup>, respectively for **ICT4:PC<sub>71</sub>BM** and **ICT6:PC<sub>71</sub>BM** based devices and are closely resembles with the values obtained from J–V characteristics (Table 3).

Hole and electron mobility of the blend films are evaluated by measuring the J–V characteristics of hole only (ITO/PEDOT:PSS/**ICT4** or **ICT6:PC<sub>71</sub>BM**/Au) and electron only (ITO/Al/**ICT4** or **ICT6:PC<sub>71</sub>BM**/Al) devices, in dark, employing space charge limited current (SCLC) model (Fig. 5). Devices with as cast **ICT4:PC<sub>71</sub>BM** and **ICT6:PC<sub>71</sub>BM** active layers shows hole mobility ( $\mu_h$ ) of  $1.16 \times 10^{-5}$  and  $4.53 \times 10^{-5}$  cm<sup>2</sup>/Vs, respectively in donor phase, while corresponding electron mobility ( $\mu_e$ ) in acceptor phase is  $2.45 \times 10^{-4}$  and  $2.52 \times 10^{-5}$  cm<sup>2</sup>/Vs, respectively. The pronounced difference between  $\mu_h$  and  $\mu_e$  indicates that holes and electrons transports are not balanced in the as cast devices. Upon TSA treatment, the hole mobility ( $\mu_h$ ) in the donor phase is increased ( $9.56 \times 10^{-5}$  and  $1.94 \times 10^{-4}$  cm<sup>2</sup>/Vs, respectively for **ICT4:PC<sub>71</sub>BM** and **ICT6:PC<sub>71</sub>BM** active layers). However, decrement in the electron mobility is observed ( $2.40 \times 10^{-4}$  cm<sup>2</sup>/Vs and  $2.48 \times 10^{-4}$  cm<sup>2</sup>/Vs, respectively **ICT4:PC<sub>71</sub>BM** and **ICT6:PC<sub>71</sub>BM** active

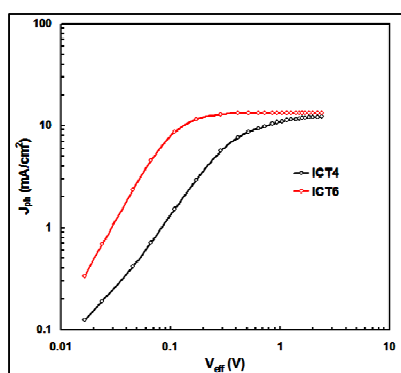
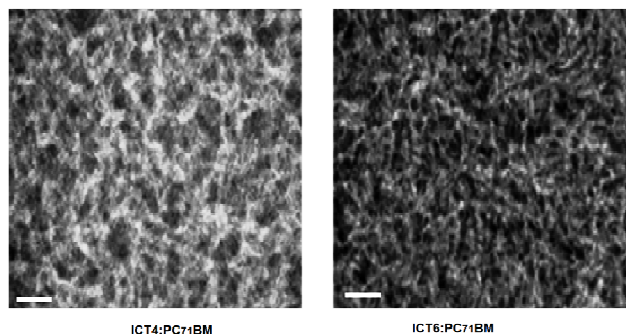


Fig. 6  $J_{ph}$  Vs  $V_{eff}$  characteristics of BHJSCs with TSA treated **ICT4:PC<sub>71</sub>BM** and **ICT6:PC<sub>71</sub>BM** active layers

layers) leading to more balanced charge transport. The blend film of **ICT6** based active layers (both as cast and TSA treated) has higher hole mobilities than **ICT4** counterpart. This property leads to better charge extraction and hence to higher  $J_{SC}$  and FF of the BHJSCs.<sup>25</sup> Higher IPCE and  $J_{SC}$  values of **ICT6** based device compared to **ICT4** are attributed to rapid exciton dissociation in blended active layer as confirmed by the PL spectra (Fig. S8b, ESI<sup>†</sup>) and efficient charge transport as evidenced by the hole mobility. These results suggest that substitution of fluorine atoms onto the BT units of donor molecule can enhance intermolecular charge transport in the BHJ active layer.

Further, improved performance of BHJSCs with **ICT6** donor and its significant difference from **ICT4** counterparts is supported by photocurrent density ( $J_{ph}$ ,  $J_{ph} = J_L - J_D$ , where  $J_D$  and  $J_L$  are the current densities in dark and under illumination, respectively) and effective voltage ( $V_{eff}$ ,  $V_{eff} = V_o - V_{app}$ , where  $V_o$  is the voltage at zero  $J_{ph}$  and  $V_{app}$  is the voltage applied) characteristics. The plots of  $J_{ph}$  Vs  $V_{eff}$  for the BHJSCs are presented in Fig. 6. In the case of **ICT6** based device, at low value of  $V_{eff}$ ,  $J_{ph}$  has nearly linear dependence on voltage and  $J_{ph}$  starts to reach saturation at  $V_{eff}$  around 0.64 V and fully saturated at  $V_{eff} = 2.4$  V. This indicates that photogenerated excitons are effectively dissociated and the generated free charge carriers are efficiently collected at electrodes with minute germinate or bimolecular recombination. But, for the **ICT4** based device,  $J_{ph}$  has greater field dependence over a larger bias range and  $J_{ph}$  is not saturated fully even at  $V_{eff} = 2.4$  V, indicating considerable germinate and /or bimolecular recombination and poor extraction/collection of charge carriers at electrodes. Efficient charge dissociation and effective charge collection at electrodes could improve the FF values of the BHJSCs with **ICT6** over its **ICT4** counterpart.<sup>60,61</sup> The ratio of  $J_{ph}/J_{sat}$  can represent the overall exciton dissociation efficiency.<sup>62</sup> The  $J_{ph}/J_{sat}$  ratios for the BHJSCs based on **ICT4** and **ICT6** measured under short circuit conditions, are 0.86 and 0.93, respectively. Higher  $J_{ph}/J_{sat}$  ratio of **ICT6** based BHJSCs indicates efficient exciton dissociation for **ICT6** based device compared to the device with **ICT4** active layer. At maximal power output conditions,  $J_{ph}/J_{sat}$  is 0.66 and 0.70 for **ICT4** and **ICT6** based devices, respectively and it also indicates higher charge collection efficiency and suppressed bimolecular recombination for the **ICT6** based BHJSC devices. Series resistance ( $R_s$ ) and shunt resistance ( $R_{sh}$ ) of the **ICT4** and **ICT6** based BHJSCs are calculated from the inverse slope near  $V_{oc}$  and  $J_{sc}$  of the J–V characteristics of the respective devices under illumination, respectively. Compared to the device with **ICT4** ( $R_s = 12.56 \Omega \text{ cm}^2$ ), the device with **ICT6** ( $R_s = 5.34 \Omega \text{ cm}^2$ ) shows smaller  $R_s$ , indicating that decrease in the hole collection barrier at the anode interfaces induced by the more favorable nanoscale morphology and vertical phase separation as observed in TEM images. The observed decrease in  $R_s$  and increase in  $R_{sh}$  values for **ICT6** based device also reflect the better PCE of **ICT6**, supports better charge transport and efficient charge extraction by the electrodes. As we have adopted same device structure and processing treatment procedure, observed superiority in the photovoltaic properties of the **ICT6** based BHJSCs could be due



**Fig. 7.** Transmission electron microscopy (TEM) images of TSA treated **ICT4:PC<sub>71</sub>BM** and **ICT6:PC<sub>71</sub>BM** thin films, bar is 100 nm

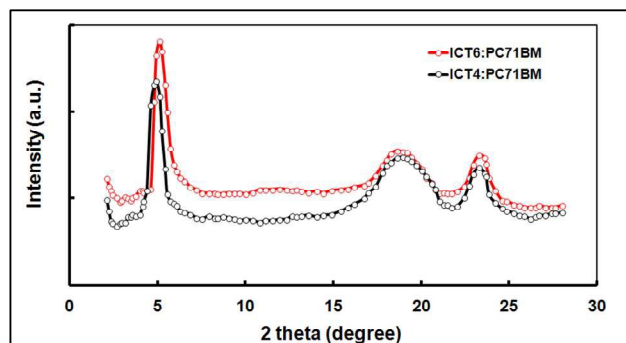


**Fig. 8.** X-ray diffraction of TSA treated **ICT4:PC<sub>71</sub>BM** and **ICT6:PC<sub>71</sub>BM** blend thin films

to its structure driven favorable active layer morphology. For efficient exciton dissociation and charge transport, morphology of the BHJ should be bi-continuous, interpenetrating with large interfacial area and regular nanoscale D/A phase separation (domain size 10-20 nm).<sup>63,64</sup> To get information about the morphology of the BHJ, we have performed transmission electron microscopy (TEM) and X-ray diffraction (XRD) analyses on TSA processed **ICT4:PC<sub>71</sub>BM** and **ICT6:PC<sub>71</sub>BM** active layers. The TEM images of the active layers processed with TSA treatment are presented in **Fig. 7**. The bright and dark regions in the TEM images correspond to the small molecule donor (**ICT4** or **ICT6**) and **PC<sub>71</sub>BM** domains, respectively. As shown in **Fig. 7**, **ICT6:PC<sub>71</sub>BM** blend film exhibits more appropriate nanoscale morphology and phase separation than **ICT4:PC<sub>71</sub>BM** counterpart, leading to more effective charge separation at D/A interface. This result indicates that the fluorination would induce better compatibility between **ICT6** and **PC<sub>71</sub>BM** due to the weak interaction from fluorine atom in the BT unit.<sup>65</sup> This favorable nanoscale morphology can facilitate exciton dissociation and charge transport and affords a higher  $J_{sc}$  and FF values to the corresponding BHJSCs. Favorable vertical phase separation and nanoscale morphology observed for **ICT6:PC<sub>71</sub>BM** active layer compared to **ICT4:PC<sub>71</sub>BM** may also be related to decrease in  $R_s$ . However the nanoscale morphology of the as cast active layer is effectively poor (as shown in Fig. S14, ESI<sup>†</sup>), leading to the charge transport and low FF, resulting lower overall PCE for OSC based on as cast film. XRD patterns of TSA treated **ICT4:PC<sub>71</sub>BM** and **ICT6:PC<sub>71</sub>BM** films are presented in **Fig. 8** and XRD patterns of as cast blend films based on **ICT4:PC<sub>71</sub>BM** and **ICT6:PC<sub>71</sub>BM** are also shown in Fig. S15, ESI<sup>†</sup>. The as cast active layer film showed a broad diffraction peak at  $2\theta = 4.96^\circ$  and  $5.14^\circ$  corresponding to (100) d-spacing. The broad diffraction peak indicates that the as cast films exhibit poor crystallinity. However, after TSA treatment the intensity of diffraction peak of the active layer films is increased considerably, indicating that the crystallinity of the active layer increased. The TSA treated active layer thin films shows a diffraction peak at  $2\theta = 4.96^\circ$  and  $5.14^\circ$ , corresponding to the inter-chain separation (d-spacing) of 1.56 nm and 1.45 nm, respectively for

**ICT4:PC<sub>71</sub>BM** and **ICT6:PC<sub>71</sub>BM** and it could be originated from the small crystalline domains of **ICT4** and **ICT6**.<sup>66</sup> Although both the small molecules possess same side chains, the intensity of (100) diffraction peak of **ICT6** is higher with shorter d-spacing value compared to **ICT4**.<sup>67,68</sup> This indicates that **ICT6** has improved lamellar stacking structure due to the self assembly induced by the fluorine atoms of F2BT units during the film formation.<sup>58</sup> In both the blend films, a broad scattering at  $2\theta = 18.62^\circ$  and a reflection peak at  $2\theta = 23.26^\circ$  are observed. The broad scattering band at  $2\theta = 18.62^\circ$  could be originating from the amorphous **PC<sub>71</sub>BM** agglomerate regions and reflection peak at  $2\theta = 23.26^\circ$  corresponds to (010) reflection of the donor materials.<sup>67,68</sup> The coherence lengths for these blend films are estimated from the Scherrer's equation and are found to be 4.17 nm and 4.58 nm for **ICT4:PC<sub>71</sub>BM** and **ICT6:PC<sub>71</sub>BM**, respectively. It can be seen from **Fig. 8** that the intensity of both (100) and (010) reflection peaks for **ICT6** are significantly higher than **ICT4** indicating that fluorinated BT in the backbone preferably adopted a face on orientation towards the substrate with high degree of lamellar ordering and  $\pi$ - $\pi$  stacking. Therefore, we assume that fluorination of small molecule donor (**ICT6**) can enhance the inter-chain  $\pi$ - $\pi$  stacking attributed to relatively high co-planarity of the molecular backbone induced by the intermolecular interactions. These results indicate that in fluorinated small molecule, the 'H' to 'F' exchange in the molecule backbone promotes intermolecular interaction and packing and it is presumably because of the lower steric effect of fluorine atoms present in **ICT6**. The stronger intensity of the (100) peak for **ICT6** in the blend film than that for **ICT4** indicates that the crystallinity of former is higher than that for later. As a result, charge transport is enhanced through the strong  $\pi$ - $\pi$  stacking interaction, compact  $\pi$ - $\pi$  stacking and high crystalline nature which are in line with the hole mobilities values obtained from SCLC measurements. Hence these results collectively supports that fluorine atom substitution on the donor materials molecular backbone can induce favorable morphology to the BHJ due to the increase inter-chain interaction of small molecule leading to different molecular packing behavior in the films thereby enhance exciton dissociation, charge transport, charge collection efficiency and suppress

bimolecular recombination of the BHJSCs, leading to the higher PCE of the resultant devices.

## Conclusion

Two novel, D<sub>1</sub>-A-D<sub>2</sub>-A-D<sub>1</sub> structured, small molecule donor materials (**ICT4** and **ICT6**) with variations in the number of fluorine atoms on the acceptor moieties (BT for **ICT4** and F2BT for **ICT6**) are synthesized and explored its effect on the optical, electronic and photovoltaic properties of the donor materials. BHJSCs are fabricated using **ICT4/ICT6** donor and PC<sub>71</sub>BM acceptor materials. BHJSCs with **ICT6**:PC<sub>71</sub>BM active layer processed with TSA (PCE = 7.91 %, J<sub>sc</sub> = 12.23 mA/cm<sup>2</sup>, V<sub>oc</sub> = 0.98 V and FF = 0.66) shows superior photovoltaic performance over the device with **ICT4**:PC<sub>71</sub>BM active layer (PCE = 5.46 %, J<sub>sc</sub> = 10.52 mA/cm<sup>2</sup>, V<sub>oc</sub> = 0.91 V and FF = 0.57). Increasing the number of fluorine atoms significantly lowers down the HOMO level of the donor material and improves the V<sub>oc</sub> of BHJSCs. It also enhances the intermolecular interaction among the donor materials in their active layer thin films and results in better hole mobility (9.56 × 10<sup>-5</sup> and 1.94 × 10<sup>-4</sup> cm<sup>2</sup>/Vs, respectively for **ICT4**:PC<sub>71</sub>BM and **ICT6**:PC<sub>71</sub>BM active layers) and balanced charge transport. Further, fluorine atoms on the acceptor moiety (F2BT) of **ICT6**, induce favorable nanoscale morphology to **ICT6**:PC<sub>71</sub>BM active layer resulting improved exciton dissociation, charge transport, charge collection efficiency and reduces bimolecular recombination of the BHJSCs. Reported PCE (7.91 %) of the BHJSCs with **ICT6** donor is one among the best reported for BT based donor materials.

## Acknowledgements

N.R. Cherreddy thanks the DST, India, for INSPIRE faculty Fellowship. B.M. Reddy and B. Shanigaram thank the UGC and CSIR, India, for research fellowship. Financial support from CSIR project NWP0054 is greatly acknowledged.

## Electronic Supplementary Information (ESI†)

NMR, MALDI-MS, absorption and emission spectra and theoretical calculations are provided in ESI†.

## Notes and references

- 1 A. J. Heeger, *Chem. Soc. Rev.*, 2010, **39**, 2354.
- 2 Y. Li, *Acc. Chem. Res.*, 2012, **45**, 723.
- 3 F. C. Krebs, *Sol. Energy Mater. Sol. Cells*, 2009, **93**, 394.
- 4 Y. Liu, J. Zhao, Z. Li, C. Mu, W. Ma, H. Hu, J. Jiang, H. Lin, H. Ade and H. Yan, *Nat. Commun.*, 2014, **5**, 5293.
- 5 Z. He, B. Xiao, F. Liu, H. Wu, Y. Yang, S. Xiao, C. Wang, T. P. Russell and Y. Cao, *Nat. Photonics*, 2015, **9**, 174.
- 6 Z. Zheng, S. Zhang, M. Zhang, K. Zhao, L. Ye, Y. Chen, B. Yang and J. Hou, *Adv. Mater.*, 2015, **27**, 1189.
- 7 H. Yao, W. Zhao, Z. Zheng, Y. Cui, J. Zhang, Z. Wei and J. Hou, *J. Mater. Chem. A*, 2016, **4**, 1708.
- 8 C. C. Chen, W. H. Chang, K. Yoshimura, K. Ohya, J. You, J. Gao, Z. Hong and Y. Yang, *Adv. Mater.*, 2014, **26**, 5670.

- 9 H. Zhou, Y. Zhang, C. K. Mai, S. D. Collins, G. C. Bazan, T. Q. Nguyen and A. J. Heeger, *Adv. Mater.*, 2015, **27**, 1767.
- 10 Y. Liu, X. Wan, F. Wang, J. Zhou, G. Long, J. Tian, J. You, Y. Yang and Y. Chen, *Adv. Energy Mater.*, 2011, **1**, 771.
- 11 J. Zhou, Y. Zuo, X. Wan, G. Long, Q. Zhang, W. Ni, Y. Liu, Z. Li, G. He, C. Li, B. Kan, M. Li and Y. Chen, *J. Am. Chem. Soc.*, 2013, **135**, 8484.
- 12 L. Dou, J. You, Z. Hong, Z. Xu, G. Li, R. A. Street and Y. Yang, *Adv. Mater.*, 2013, **25**, 6642.
- 13 Q. Zhang, B. Kan, F. Liu, G. Long, X. Wan, X. Chen, Y. Zuo, W. Ni, H. Zhang, M. Li, Z. Hu, F. Huang, Y. Cao, Z. Liang, M. Zhang, T. P. Russell and Y. Chen, *Nat. Photonics*, 2014, **9**, 35.
- 14 Y. Liu, C.-C. Chen, Z. Hong, J. Gao, Y. Yang, H. Zhou, L. Dou, G. Li and Y. Yang, *Sci. Rep.*, 2013, **3**, 3356.
- 15 Y. Patil, R. Misra, M. K. Singh and G. D. Sharma, *Phys. Chem. Chem. Phys.*, 2017, **19**, 7262.
- 16 Y. Patil, R. Misra, F. C. Chen and G. D. Sharma, *Phys. Chem. Chem. Phys.*, 2016, **18**, 22999.
- 17 P. Gautam, R. Misra, S. Biswas and G. D. Sharma, *Phys. Chem. Chem. Phys.*, 2016, **18**, 13918.
- 18 P. Gautam, R. Misra and G. D. Sharma, *Phys. Chem. Chem. Phys.*, 2016, **18**, 7235.
- 19 T. Jadhav, R. Misra, S. Biswas and G. D. Sharma, *Phys. Chem. Chem. Phys.*, 2015, **17**, 26580.
- 20 P. Gautam, R. Sharma, R. Misra, M. L. Keshtov, S. A. Kuklin and G. D. Sharma, *Chem. Sci.*, 2017, **8**, 2017.
- 21 Y. Patil, R. Misra, M. L. Keshtov and G. D. Sharma, *J. Mater. Chem. A*, 2017, **5**, 3311.
- 22 G. D. Sharma, Y. Patil, R. Misra and R. Singhal, *J. Mater. Chem. A*, DOI 10.1039/C7TA03322B.
- 23 H. Chen, J. Hou, S. Zhang, Y. Liang, G. Yang, Y. Yang, L. Yu, Y. Wu and G. Li, *Nat. Photonics*, 2009, **3**, 649.
- 24 K. Vandewal, K. Tvingstedt, A. Gadisa, O. Inganäs and J. V. Manca, *Nat. Mater.*, 2009, **8**, 904.
- 25 M. R. Busireddy, V. Mantena, N. R. Cherreddy, B. Shanigaram, B. Kotamarthi, S. Biswas, G. D. Sharma and J. R. Vaidya, *Org. Electron.*, 2016, **37**, 312.
- 26 M. R. Busireddy, V. Mantena, N. R. Cherreddy, B. Shanigaram, B. Kotamarthi, S. Biswas, G. D. Sharma and J. R. Vaidya, *Phys. Chem. Chem. Phys.*, 2016, **18**, 32096.
- 27 W. Li, S. Albrecht, L. Yang, S. Roland, J. R. Tumbleston, T. McAfee, L. Yan, M. A. Kelly, H. Ade, D. Neher and W. You, *J. Am. Chem. Soc.*, 2014, **136**, 15566.
- 28 H. Bronstein, J. M. Frost, A. Hadipour, Y. Kim, C. B. Nielsen, R. S. Ashraf, B. P. Rand, S. Watkins and I. McCulloch, *Chem. Mater.*, 2013, **25**, 277.
- 29 B. Carsten, J. M. Szarko, H. J. Son, W. Wang, L. Lu, F. He, B. S. Rolczynski, S. J. Lou, L. X. Chen and L. Yu, *J. Am. Chem. Soc.*, 2011, **133**, 20468.
- 30 B. S. Rolczynski, J. M. Szarko, H. J. Son, Y. Liang, L. Yu and L. X. Chen, *J. Am. Chem. Soc.*, 2012, **134**, 4142.
- 31 H. S. Lee, H. G. Song, H. Jung, M. H. Kim, C. Cho, J. Y. Lee, S. Park, H. J. Son, H. J. Yun, S. K. Kwon, Y.-H. Kim and B. Kim, *Macromolecules*, 2016, **49**, 7844.
- 32 T. Umeyama, Y. Watanabe, E. Douvogianni and H. Imahori, *J. Phys. Chem. C*, 2013, **117**, 21148.
- 33 S. Albrecht, S. Janietz, W. Schindler, J. Frisch, J. Kurpiers, J. Kniepert, S. Inal, P. Pingel, K. Fostiropoulos, N. Koch and D. Neher, *J. Am. Chem. Soc.*, 2012, **134**, 14932.
- 34 Y. Zhang, J. Zou, C. C. Cheuh, H. L. Yip and A. K.-Y. Jen, *Macromolecules*, 2012, **45**, 5427.
- 35 L. Cartwright, A. Iraqi, Y. Zhang, T. Wang and D. G. Lidzey, *RSC Adv.*, 2015, **5**, 46386.
- 36 Z. Li, J. Lu, S.-C. Tse, J. Zhou, X. Du, Y. Tao and J. Ding, *J. Mater. Chem.*, 2011, **21**, 3226.
- 37 Y. Zhang, S. C. Chien, K.-S. Chen, H.-L. Yip, Y. Sun, J. A. Davies, F.-C. Chen and A. K.-Y. Jen, *Chem. Commun.*, 2011, **47**, 11026.

## ARTICLE

Journal Name

- 38 J. Kim, M. H. Yun, G.-H. Kim, J. Lee, S. Lee, M. S. J. Ko, Y. Kim, G. K. Dutta, M. Moon, S. Y. Park, D. S. Kim, J. Y. Kim and C. Yang, *ACS Appl. Mater. Interfaces*, 2014, **6**, 7523.
- 39 N. Wang, Z. Chen, W. Wei and Z. Jiang, *J. Am. Chem. Soc.*, 2013, **135**, 17060.
- 40 B. C. Schroeder, Z. Huang, R. S. Ashraf, J. Smith, P. D'Angelo, S. E. Watkins, T. D. Anthopoulos, J. R. Durrant and I. McCulloch, *Adv. Funct. Mater.*, 2012, **22**, 1663.
- 41 J. Lee, M. Jang, S. M. Lee, D. Yoo, T. J. Shin, J. H. Oh and C. Yang, *ACS Appl. Mater. Interfaces.*, 2014, **6**, 20390.
- 42 J. W. Jo, J. W. Jung, E. H. Jung, H. Ahn, T. J. Shin and W. H. Jo, *Energy Environ. Sci.*, 2015, **8**, 2427.
- 43 J. L. Wang, Q.-R. Yin, J.-S. Miao, Z. Wu, Z.-F. Chang, Y. Cao, R.-B. Zhang, J.-Y. Wang, H.-B. Wu and Y. Cao, *Adv. Funct. Mater.*, 2015, **25**, 3514.
- 44 J. J. Intemann, K. Yao, F. Ding, Y. Xu, X. Xin, X. Li and A. K.-Y. Jen, *Adv. Funct. Mater.*, 2015, **25**, 4889.
- 45 S. Paek, N. Cho, K. Song, M.-J. Jun, J. K. Lee and J. Ko, *J. Phys. Chem. C*, 2012, **116**, 23205.
- 46 X. Liao, F. Wu, L. Zhang, L. Chen and Y. Chen, *Polym. Chem.*, 2015, **6**, 7726.
- 47 X. Liu, Y. Sun, B. B. Y. Hsu, A. Lorbach, L. Qi, A. J. Heeger and G. C. Bazan, *J. Am. Chem. Soc.*, 2014, **136**, 5697.
- 48 Q.-R. Yin, J.-S. Miao, Z. Wu, Z.-F. Chang, J.-L. Wang, H.-B. Wu and Y. Cao, *J. Mater. Chem. A*, 2015, **3**, 11575.
- 49 L. Wang, L. Yin, C. Ji and Y. Li, *Dyes Pigm.*, 2015, **118**, 37.
- 50 J. Yuan, X. Huang, F. Zhang, J. Lu, Z. Zhai, C. Di, Z. Jiang and W. Ma, *J. Mater. Chem.*, 2012, **22**, 22734.
- 51 H. Zhou, L. Yang, A. C. Stuart, S. C. Price, S. Liu and W. You, *Angew. Chem. Int. Ed.*, 2011, **50**, 2995.
- 52 Y. Liu, X. Wan, F. Wang, J. Zhou, G. Long, J. Tian and Y. Chen, *Adv. Mater.*, 2011, **23**, 5387.
- 53 S. Shen, P. Jiang, C. He, J. Zhang, P. Shen, Y. Zhang, Y. Yi, Z. Zhang, Z. Li and Y. Li, *Chem. Mater.*, 2013, **25**, 2274.
- 54 C. Muller, *Chem. Mater.*, 2015, **27**, 2740.
- 55 P. Boufflet, Y. Han, Z. Fei, N. D. Treat, R. Li, D.-M. Smilgies, N. Stingelin, T. D. Anthopoulos and M. Heeney, *Adv. Funct. Mater.*, 2015, **25**, 7038.
- 56 H. J. Son, W. Wang, T. Xu, Y. Liang, Y. Wu, G. Li and L. Yu, *J. Am. Chem. Soc.*, 2011, **133**, 1885.
- 57 C. B. Nielsen, A. J. P. White and I. McCulloch, *J. Org. Chem.*, 2015, **80**, 5045.
- 58 K. Srinivas, Ch. Prabhakar, C. L. Devi, K. Yesudas, K. Bhanuprakash and V. J. Rao, *J. Phys. Chem. A*, 2007, **111**, 3378.
- 59 C. W. Tang, *Appl. Phys. Lett.*, 1986, **48**, 183.
- 60 M. M. Mandoc, W. Veurman, L. J. A. Koster, B. de Boer and P. W. Blom, *Adv. Funct. Mater.*, 2007, **17**, 2167.
- 61 C. M. Proctor, C. Kim, D. Neher and T.-Q. Nguyen, *Adv. Funct. Mater.*, 2013, **23**, 3584.
- 62 Z. He, C. Zhong, X. Huang, W.-Y. Wong, H. Wu, L. Chen, S. Su and Y. Cao, *Adv. Mater.*, 2011, **23**, 4636.
- 63 Y. Tamai, H. Ohkita, H. Benten and S. Ito, *J. Phys. Chem. Lett.*, 2015, **6**, 3417.
- 64 P. W. M. Blom, V. D. Mihailetchi, L. J. A. Koster and D. E. Markov, *Adv. Mater.*, 2007, **19**, 1551.
- 65 Z. Wang, X. Xu, Z. Li, K. Feng, K. Li, Y. Li and Q. Peng, *Adv. Electron. Mater.*, 2016, **2**, 1600061.
- 66 J. Huang, C. Zhan, X. Zhang, Y. Zhao, Z. Lu, H. Jia, B. Jiang, J. Ye, S. Zhang, A. Tang, Y. Liu, Q. Pei and J. Yao, *ACS Appl. Mater. Interfaces*, 2013, **5**, 2033.
- 67 J. Wan, X. Xu, G. Zhang, Y. Li, K. Feng and Q. Peng, *Energy Environ. Sci.*, 2017, DOI:10.1039/C7EE00805H.
- 68 A. Mishra, M. L. Keshtov, A. Looser, R. Singhal, M. Stolte, F. Würthner, P. Bäuerle and G. D. Sharma, *J. Mater. Chem. A*, DOI: 10.1039/C7TA04703G.

## Graphical Abstract

Study on the effect of fluorine substitution on the photovoltaic properties of dithieno[3,2-*b*:2',3'-*d*]pyrrole-benzo[*c*][1,2,5]thiadiazole conjugate small molecule donor materials

Manohar Reddy Busireddy,<sup>a</sup> Narendra Reddy Chereddy,<sup>a,\*</sup> Balaiah Shanigaram,<sup>b</sup> Kotamarthi Bhanuprakash,<sup>b,\*</sup> Subhayan Biswas,<sup>c</sup> Ganesh Datt Sharma<sup>c,\*</sup> Vaidya Jayathirtha Rao<sup>a,d,\*</sup>

<sup>a</sup>*Crop Protection Chemicals Division, CSIR-Indian Institute of Chemical Technology, Hyderabad-500007, India.*

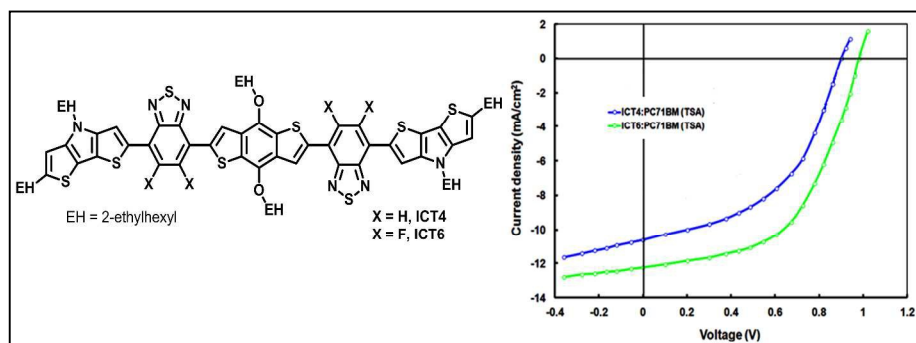
<sup>b</sup>*Inorganic and Physical Chemistry Division, CSIR-Indian Institute of Chemical Technology, Hyderabad-500007, India.*

<sup>c</sup>*Department of Physics, The LNM Institute of Information Technology, Jamdoli, Jaipur, India.*

<sup>d</sup>*AcSIR, CSIR-Indian Institute of Chemical Technology, Hyderabad-500007, India.*

Corresponding author Tel.: +91 40 27193933; Fax: +91 40 27193382

E-Mail: [chereddynarendra@gmail.com](mailto:chereddynarendra@gmail.com) (Narendra Reddy Chereddy); [vaidya.opv@gmail.com](mailto:vaidya.opv@gmail.com) (Vaidya Jayathirtha Rao); [gdsharma273@gmail.com](mailto:gdsharma273@gmail.com) (Ganesh Datt Sharma); [bhanu2505@yahoo.co.in](mailto:bhanu2505@yahoo.co.in) (Kotamarthi Bhanuprakash)



Two novel dithieno[3,2-*b*:2',3'-*d*]pyrrole tethered, benzo[*c*][1,2,5]thiadiazole based small molecules (**ICT4** and **ICT6**) are synthesized and successfully applied as donor materials for BHJSCs with ITO/PEDOT:PSS/donor:PC<sub>71</sub>BM/PFN/Al structure. By adopting simple fabrication procedures, PCE of 5.46 % and 7.91 %, respectively achieved for BHJSCs with **ICT4** and **ICT6** donors. Importance of fluorination on the donor materials backbone to improve the photovoltaic parameters of the corresponding BHJSCs is described in detail.